1. Supplemental Information – Glacier Model

1.1. Glacier Model Overview

This model uses a finite-element numerical model from (Kessler et al., 2006) where ice accumulation and movement on a given terrain surface is governed by explicit equations for ice flux and mass conservation. The mass balance is the combination of a prescribed annual accumulation and calculated annual melt. Melt is approximated using a positive degree-day method with an additional factor to account for melt from solar radiation. The model is subsequently calibrated to observed ice limits and transient scenarios are run to explore climate sensitivity and the required climate forcings needed to reconstruct Divide Ice Cap activity over the last ~2000 years. This supplement provides details on model design, parameter selection and calibration, sensitivity analysis, and characterization of uncertainty.

2. Glacier Model Setup

2.1. Terrain Production

Prior to model implementation, a terrain model of the bedrock surface is required. This involves removing (to the best approximation) the modern Divide Ice Cap from an existing digital elevation product. ASTER digital elevation data from 2011 CE was used as a base for the two-dimensional terrain model, resampled to a 60 m pixel size. The ASTER data product was retrieved from the online Data Pool, courtesy of the NASA Land Processes Distributed Active Archive Center (LP DAAC), USGS/Earth Resources Observation and Science (EROS) Center, Sioux Falls, South Dakota, https://lpdaac.usgs.gov/data_access/data_pool. The resulting surface was smoothed using a 7x7 mean filter to remove artifacts in the raw data that would lead to instabilities in the model. Modern ice, including Divide Ice Cap and the ice on the surrounding summits, had to be removed to create an ice-free terrain to model upon. Using the best approximation of basal shear stress (τ_b) to be ~100 kPa (Haeberli, 2016), current ice thicknesses (H) were calculated following Cuffey and Paterson (2010):

$$H = \frac{\tau_b}{\rho g \theta}$$

where ρ is the density of ice (917 kg m^{-3}), g is gravitational acceleration (9.81 m s^{-2}) and θ is the surface slope of the modern ice surface. Calculated thicknesses were then subtracted from the modern terrain surface to produce an ice-free surface. Eventual model runs show that calculated and modeled modern ice thickness are the same within 10% of each other.

2.2. Mass Balance

Kessler et al. (2006) drove ice formation with a climate dictated by an equilibrium line altitude (ELA), a mass balance gradient with elevation, and a maximum positive balance (maximum accumulation). However, the overall low accumulation rates of our high-latitude site and the variable aspect of the Divide Ice Cap, which increases the influence of solar radiation during the melt season, necessitates a different approach (Benn and Evans, 2010). Ice core records, observational studies in the eastern Canadian Arctic, and previous modeling work suggest a maximum accumulation of 0.3 m water equivalent (m.w.e.) per year throughout the

Holocene (Hooke, 1976; Serreze et al., 1995; Anklin et al., 1998; Mair et al., 2005), which, given the limited elevation range of the Divide Ice Cap location, is applied as the annual accumulation across the whole model surface.

Although precipitation records are sparse near the study site, ice core records from the summit of the Greenland Ice Cap show that regionally, precipitation varied by only ~6% over the last 1200 years (Alley, 2004). Given the relatively low accumulation rates, summer temperature is likely the dominant driver of glacier advance and retreat at Divide Ice Cap (Koerner, 2005).

Temperature index melt models generally capture the majority of summer melt due to the strong relationship between air temperature and components of the surface energy balance (Braithwaite and Olesen, 1989; Lang and Braun, 1990), and have been successfully applied on larger scales in the eastern Canadian Arctic (Marshall and Sharp, 2009). However, the relatively low accumulation rates, small elevation range, and variable aspect and slope at Divide Ice Cap along with the asymmetric trimlines surrounding summits (Figure 1) suggests that the glacier system is sensitive to small temperature changes and that incoming solar radiation is an important factor in the overall glacier mass balance. Additionally, previous studies of the orientation of cirque glaciers on Baffin Island (Williams, 1975) and summertime snow patch distribution in the eastern Canadian arctic (Lauriol et al., 1986) emphasize the role of solar energy in enhancing melt on southerly aspects. Wind redistribution of snow could be another factor in the more positive mass balance of northerly aspect of the Divide Ice Cap. However, available meteorological wind direction data from Clyde River to the north and Iqaluit to the southwest both show the prevailing winds to be north-northwesterly (Gearheard et al., 2010; Nawri and Stewart, 2010). While these observations do not rule out the possibility that local winds at Divide Ice Cap differ, and move snow from south-facing to north-facing slopes, they strongly suggest that the dominant wind patterns cannot explain the asymmetric mass balance. In areas of overall low accumulation and relatively low relief where the snowline is only just below mountaintops, solar radiation modulated by slope and aspect can exert a strong control on the annual pattern of accumulation (Benn and Evans, 2010).

Given the above concerns regarding melt driven by temperature and solar radiation, we calculate the summer melt rate (M, mm day^{-1}) using a radiation modified positive degree day melt model for air temperatures (T) above 0°C (Hock, 2005; Jonsell et al., 2012; Kane et al., 1997):

$$M = \begin{Bmatrix} m_T(PDD) + m_R(1-\alpha)R); T > 0°\mathrm{C} \\ 0 \quad\quad ; T < 0°\mathrm{C} \end{Bmatrix}$$

The melt contribution from air temperature is calculated using the product of an degree-day melt factor (m_T, 6.3 mm day^{-1} °C^{-1}; Braithwaite, 1981) with positive-degree days (PDD) over the terrain surface. Using a prescribed sea-level mean annual temperature (MAT), a MAT at elevation is calculated using a near surface lapse rate of -4.9°C km^{-1} (Gardner et al., 2009). Annual temperature cycles are then calculated at all elevations using an amplitude of 20°C (based upon daily temperature records from Dewar Lakes meteorological data from 1959-2015) around the MAT. Integration of the portion of the curve where *T*>0°C provides the PDD for each location on the terrain surface.

Calculation of the melt contribution from radiation employs the product of a radiation melt factor (m_R, 0.036 mm day^{-1} (W m^{-2})$^{-1}$; obtained via model calibration, see below) with that portion of the incident solar radiation (*R*; W m^{-2}) that is not reflected from the surface (albedo = *a* = 0.5 (Benn and Evans, 2010)). Solar radiation (*R)* for the Divide Ice Cap latitude and elevation is calculated following Kustas et al. (1994 and Kumar et al. (1997). In this case, radiation is also modulated based on slope and aspect (Cuffey and Paterson, 2010; Hock, 2005; Kumar et al., 1997). Melt from solar radiation only takes place when *T*>0°C, which is calculated from the annual temperature cycle from the *PDD* component. Net mass balance is then calculated as the winter mass balance (accumulation) minus the summer mass balance (melt).

2.3. Modeling Ice Surfaces

Driven by the above mass balance, the model, following Kessler et al. (2006) calculates an ice surface on the supplied 2-D terrain surface using explicit equations for ice flux and mass conservation (equations 1 and 8 respectively in Kessler et al. (2006)). Using a shallow ice approximation and the recommended coefficient for Glen's flow law for polar ice of 3.5x10^{-25} Pa^{-1}s^{-1} (Cuffey and Paterson, 2010), ice discharge is driven by the shear stress associated with ice thickness and surface slope. Field observations of the highly preserved land surface, including vegetation still in growth position (Figure 1), justify a no-slip basal boundary condition. Sliding was therefore disallowed, and ice moves only by internal deformation.

3. Glacier Model Scenarios

3.1. Model Calibration

Prior to running full simulations of the last ~2000 years, the model must be calibrated for an appropriate solar radiation melt factor (m_R). Traditionally this is value is calibrated using in situ solar flux and melt rate data. However, since that information is lacking here, a different approach must be taken.

Given the transect chronology observed, the simplest (and most likely) history involves continuous ice advance (though likely at varying rates) from ~26 BCE – 1900 CE followed by modern retreat from ~1900 to present. Given this scenario, the model was calibrated to the observed transect chronology and run to maximum Holocene extent conditions (or at ~1900, culmination of the LIA) using a range of accepted m_R (Jonsell et al., 2012) values (and other parameters above). In other words, given a m_R value, the transect chronology was used to find the required temperature changes to advance ice through the observed chronology (Figure 1).

Figure 1: Divide Ice Cap showing major plant radiocarbon age constraints A, B, and C from oldest to youngest.

These Holocene maximum extent model runs were then compared to the observed maximum extent as seen through trimlines on the land surface (Figure 2) to find the best fit, and thus the approximate m_R for this study.

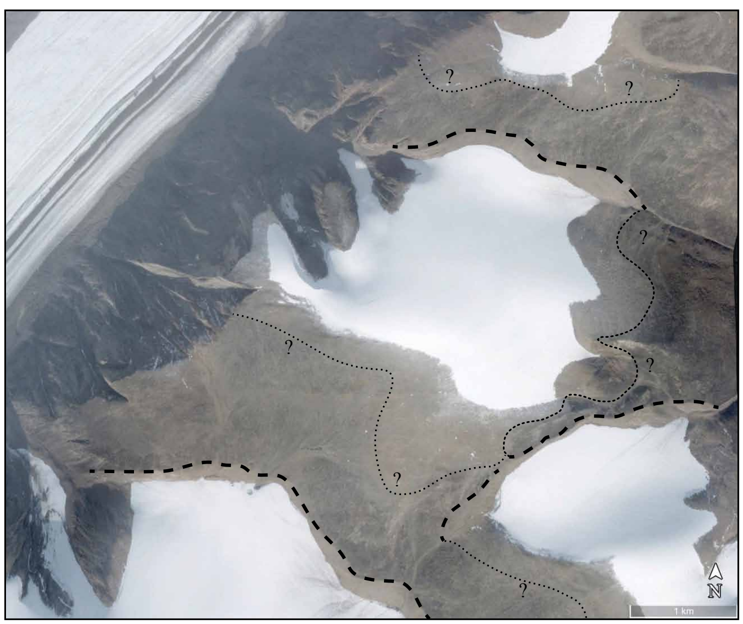

Figure 2: Satellite image of Divide Ice Cap and surround ice bodies with secure LIA trimlines (heavy dashed lines) and approximate LIA trimlines (dotted lines) show. 2011 satellite image from courtesy of Digital Globe.

With this approach we find that a m_R value of 0.036 mm day^{-1} (W m^{-2})$^{-1}$ provides the best reproduction of Holocene maximum ice extent (Figure 3). Although not a perfect match (model uncertainty discussed below), m_R values above or below this value produced far too much or too little ice (respectively), making this value our closest approximation.

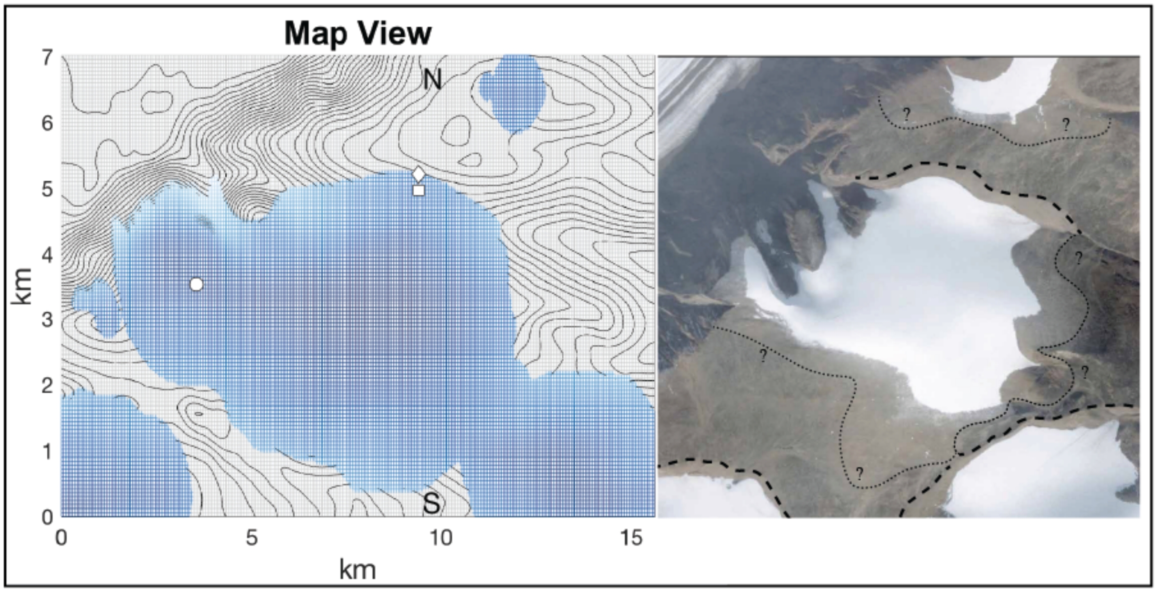

Figure 3: Map view of simulation (left panel) output showing the modeled maximum Neoglacial extent (contour interval is 30 m). Also shown is sample #12 (circle), 1000 CE margin (square), and Neoglacial maximum trimline (diamond). Right panel shows a google earth 2011 image with Neoglacial maximum extent trimlines (dashed lines) and approximate trimlines (dotted lines) shown.

3.2. *Full Simulations*

Using the calibrated model from above, it is possible to reproduce the full history of advance and retreat at Divide Ice Cap over the last ~2000 years. Beginning with ice immediately behind the oldest chronological tie-point ('A'; Figure 1), temperature was lowered to advance ice between Points 'A' and 'B' (Figure 1; ~26 BCE – 1000 CE). Temperatures were then lowered again in order to advance ice between points 'B' and 'C' (~1000 – 1910 CE; Figure 1) in order to attain the Holocene maximum configuration from above (Figure 3). Following this advance, it is possible to warm temperature and model ice cap melt of the past century. Assuming that retreat began early in the 20th century around 1910, a linear rate of warming (the simplest case) can be found that drives the ice margin back to its 2015 position in the request 105 years (Figure 4). Using the previously calibrated model, a warming rate of 0.028 °C yr^{-1} forces ice margin retreat in ~108 years, equaling a cumulative warming of ~2.8°C. Although warming at Divide Ice Cap was unlikely linear over this entire period, this model warming falls between the longer term warming at Dewar Lakes (0.0141 °C yr^{-1} from 1959-2015) and more recent warming at Qikiqtarjuaq (0.0867 °C yr^{-1} from 1995-2009). With this optimized warming trend, the full 2000-year history of Divide Ice Cap constrained by plant radiocarbon ages and observed trimlines can be reconstructed using the minimum required temperature fluctuations.

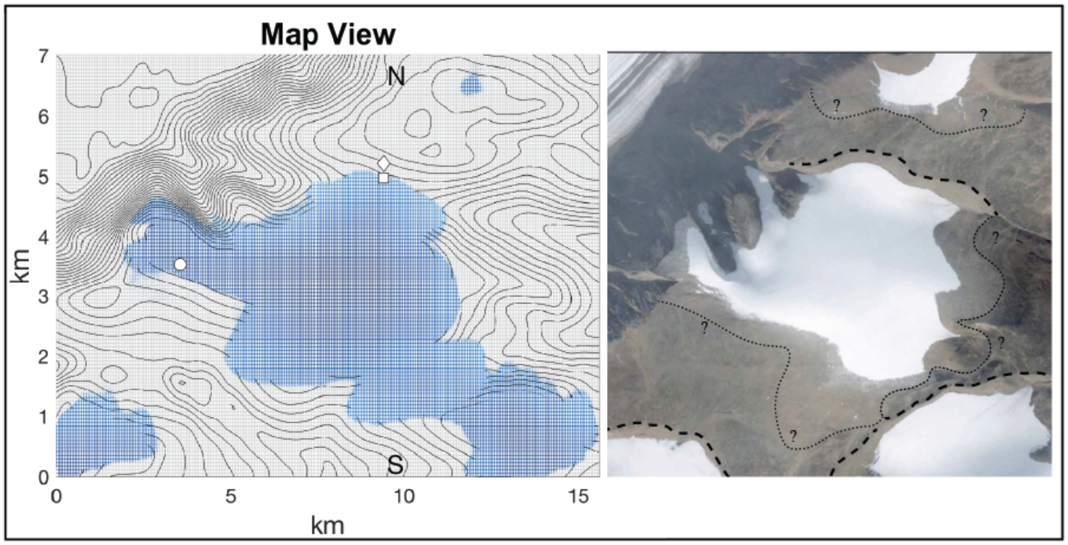

Figure 4: Final output from the full simulation model showing the modeled modern (2015 CE) extent of the ice cap following the advance and retreat scenarios outlined in text.

4. Sensitivity Analysis

Among the parameter values prescribed for this model, the uniform and constant accumulation rate is perhaps the most unrealistic and therefore could have the largest impact on the model outcome. To test model sensitivity to accumulation rate, we ran the model to completion as above using 0.2 and 0.5 m.w.e. Keeping all other parameters the same, including the solar radiation melt factor calibrated form the original run, simulations with 0.5 m.w.e. fail to reproduce the correct LIA ice configuration. This is partly due to the fact that a higher accumulation rate has a higher equilibrium line altitude (ELA) and necessitates a warmer mean annual temperature than the original scenario to accumulate snow/ice at the same elevations (the same temperature forcing with a higher accumulation rate would produce too much ice and covers the entire study area). This higher temperature increases the length of the melt season (Figure 5), therefore amplifying the influence of the solar radiation melt factor (which is only in effect when air temperature is above 0°C).

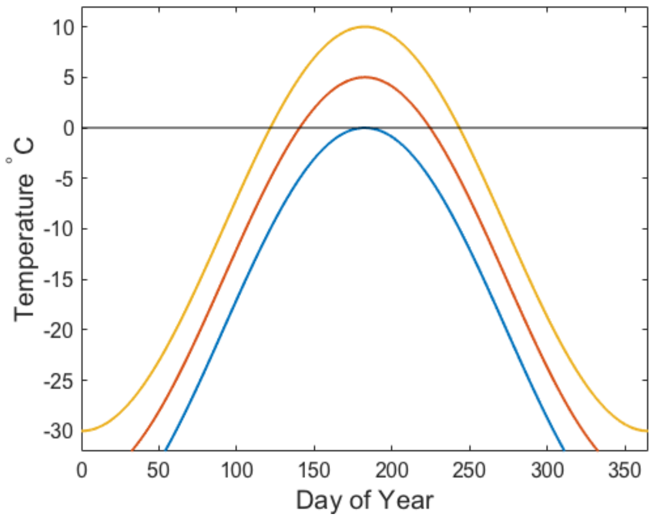

Figure 5:Modeled daily annual temperatures illustrating the changing length of melt season (portion of curve above 0°C) with changing mean annual temperature.

This then amplifies the asymmetry of ice distribution and prevents ice from advancing through the transect chronology as observed. However, when the solar melt factor is lowered to compensate for the above increase in melt season length, the only way to advance ice through the chronology in the observed time constraints is to raise temperatures during the 2nd millennium CE and through the LIA, which itself it highly unlikely. Additionally, the Holocene maximum extent from these higher accumulation and lower solar melt factor runs deviate greatly from the observed maximum extent (Figure 6).

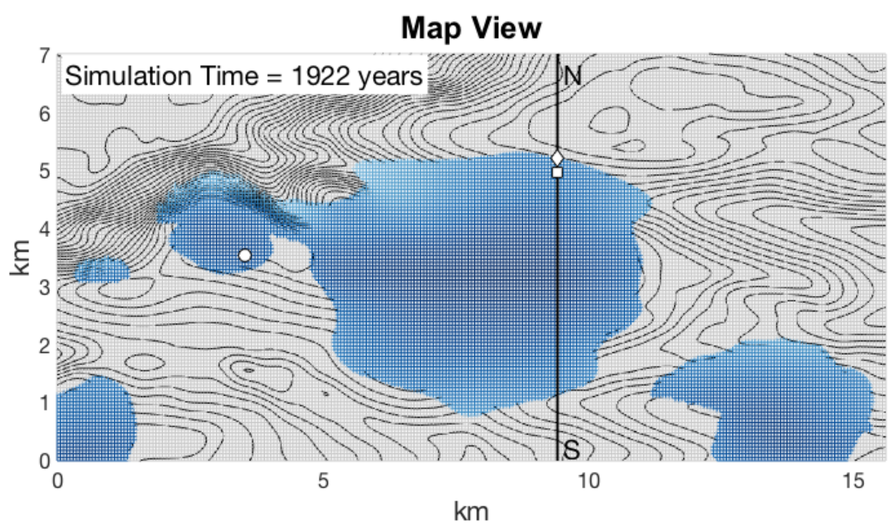

Figure 6:Maximum Holocene extent under higher accumulation rate and lower solar radiation melt factor illustrating highly asymmetric configuration deviating from observed maximum extent (Figure 2).

These results from the higher accumulation scenario suggest that indeed the accumulation rate at the study site is likely less than 0.5 m.w.e.

Conversely, a lower accumulation rate of 0.2 m.w.e. raises the ELA and thus requires slightly cooler temperatures to accumulate ice at the correct elevations. When run with the same parameter values as the original simulation we find that total minimum required cooling over the last ~2000 years increases from 0.45 to 0.5°C. This makes sense, since less accumulation would raise the ELA, then a temperature decrease is needed to lower it again. However, since cooler mean annual temperatures shorten the melt season, and lessening the influence of solar melt, model simulations with a lower accumulation rate have less asymmetry in the final ice configuration, and thus deviating from the observed Holocene maximum ice configuration (Figure 7).

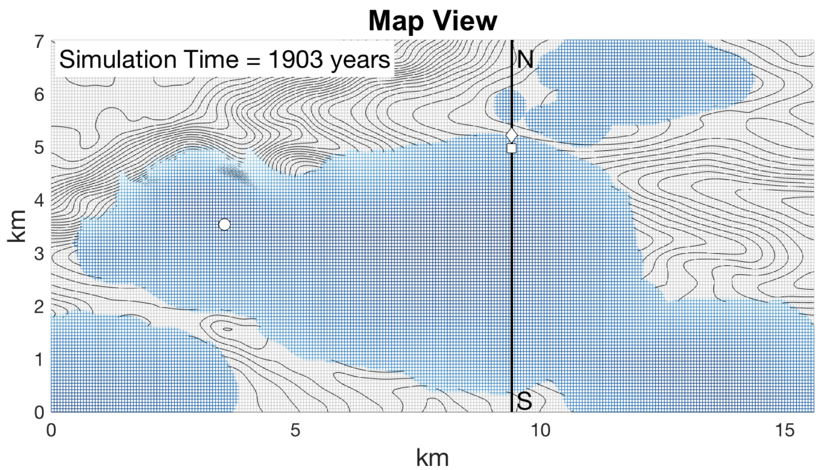

Figure 7:Modeled Holocene maximum extent for a lower accumulation and same solar radiation melt factor as original scenario. Note lack of ice cap asymmetry which fails to match the observed maximum extent

5. Glacier Model Uncertainty

In the modeling experiments used in this study, uncertainty is difficult to quantify, but it is worthwhile to acknowledge potential sources of error and uncertainty. First, though modeled ice thicknesses agreed with the thickness of modern ice removed to create an unglaciated surface, collection of subglacial topography data would greatly reduce the error here. Sensitivity analysis showed that the accumulation rate is likely fairly accurate, however, longer term records of accumulation in the region would help to reduce uncertainty with the mass balance. Additionally, in situ mass balance data, including incoming solar radiation would allow for the calibration of a local solar radiation melt factor (e.g., Jonsell et al., 2012). Additionally, wind redistribution of snow likely plays a part in the mass balance of Divide Ice cap and the asymmetry present in the Holocene maximum extent. Capturing this factor is beyond the scope of this study, but important to acknowledge. The model in this study captures the first-order trends and highlights areas of where similar future studies could benefit from additional observation and measurements to reduce error and improve model performance.

6. Comparison to Modeled Temperatures

This section describes how we utilized global climate model simulations to compare to the temperature changes for Divide Ice Cap (DIC) reported here. Otto-Bliesner et al. (2016) used the Community Earth System Model (CESM) version 1.1 with the Community

Atmospheric Model 5 (CAM 5) to produce the CESM Last Millennium Ensemble (LME). The model was branched from an 1850 CE control, spun up under 850 CE conditions, and then run to 1850 CE using orbital, solar, volcanic, changes in land use/cover and greenhouse gases forcings (see Otto-Bliesner et al., 2016 for details). On average, the 13 LME members show that the last millennium was ~0.2°C cooler than 850 CE conditions in the terrestrial region of 60-90°N and 90°W-60°E (Fig. 8), similar to the results of our DIC glacier model presented here.

In order to perform a comparison with the DIC results over the last 2 millennia, we also analyzed the ongoing *past2K* simulation with the same model version as used for the CESM LME. That simulation was initialized from the 850 CE control from Otto-Bliesner et al. (2016) and spun up for 1 CE conditions. We then ran it forward to 1850 CE using forcing compiled by the PMIP4 working group (Jungclaus et al., 2016)At the time of submission, the simulation was still running and had only reached 1270 CE. However, the simulation indicates that the first millennium CE was ~0.2°C cooler than 1 CE conditions (Fig. 8), similar to the results of the DIC glacier model presented here.

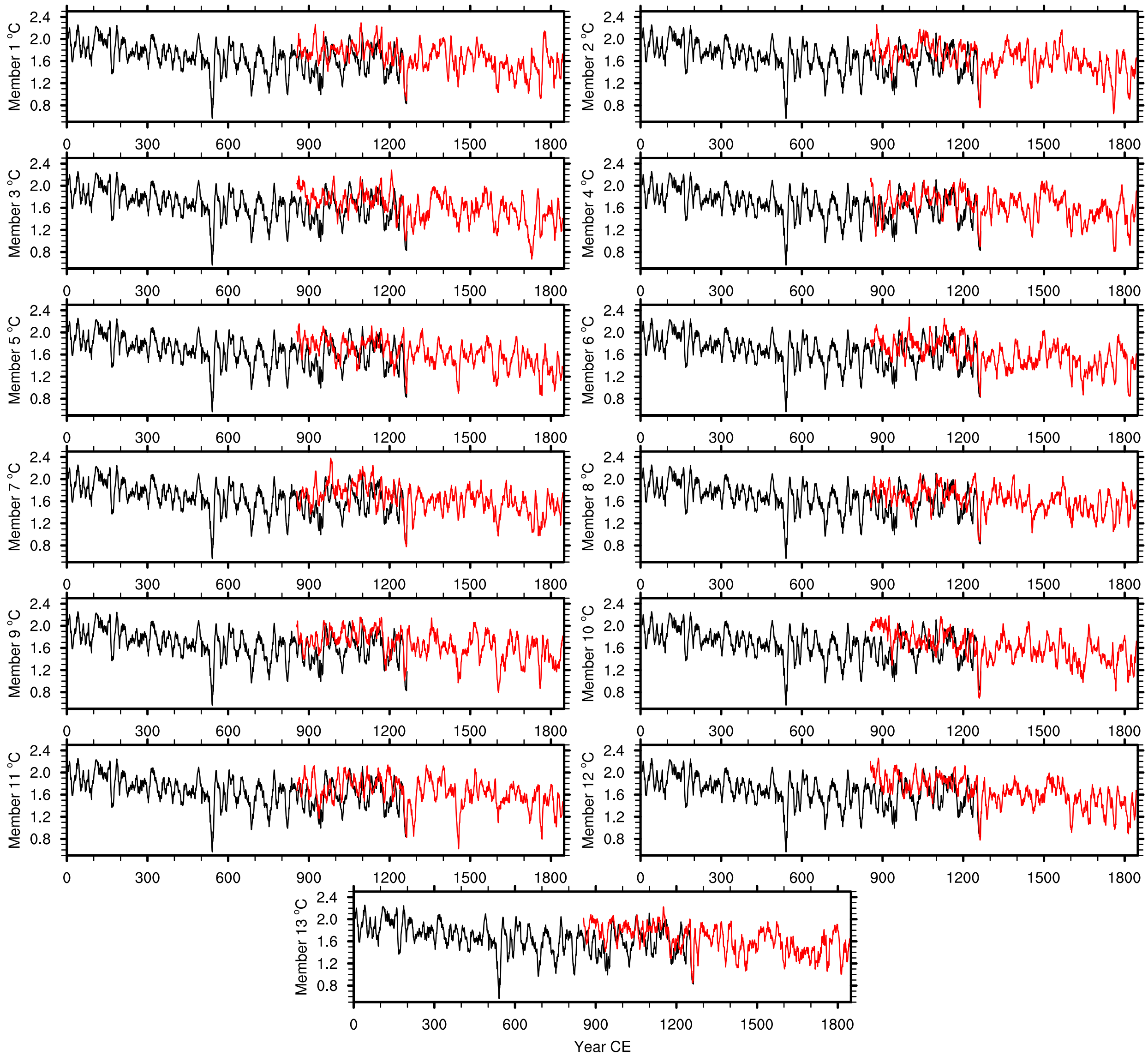

Figure 8: Simulated decadal 2 m air temperature (°C) over land during JJA in the Atlantic Arctic (90W-60E, 60N-90N) from the 13 fully-forced CESM-LME simulations (red curves) shown against the ongoing CESM past2k simulation (black curve). The simulations indicate ~0.2°C of cooling in the first and second millennium, though some offset between the simulations is apparent, likely due to the different initial conditions.

Although the full 0-1850 CE simulation was incomplete at the time of submission, it is still possible to use both the LME and ongoing simulations to estimate temperature change for the Atlantic Arctic over the past ~2000 years. The LME members and our simulation overlap between 850-1270 CE, and the mean offset between the runs approaches a steady value of +0.21°C as the years of overlap increase. The mean variance in the offset falls below 1% of initial variance as the period of overlap increases reaches ~125 years for all 13 members, meaning that our 250 years of overlap is sufficient to capture the systematic offset between our first millennium simulation and the LME simulations (Fig. 9).

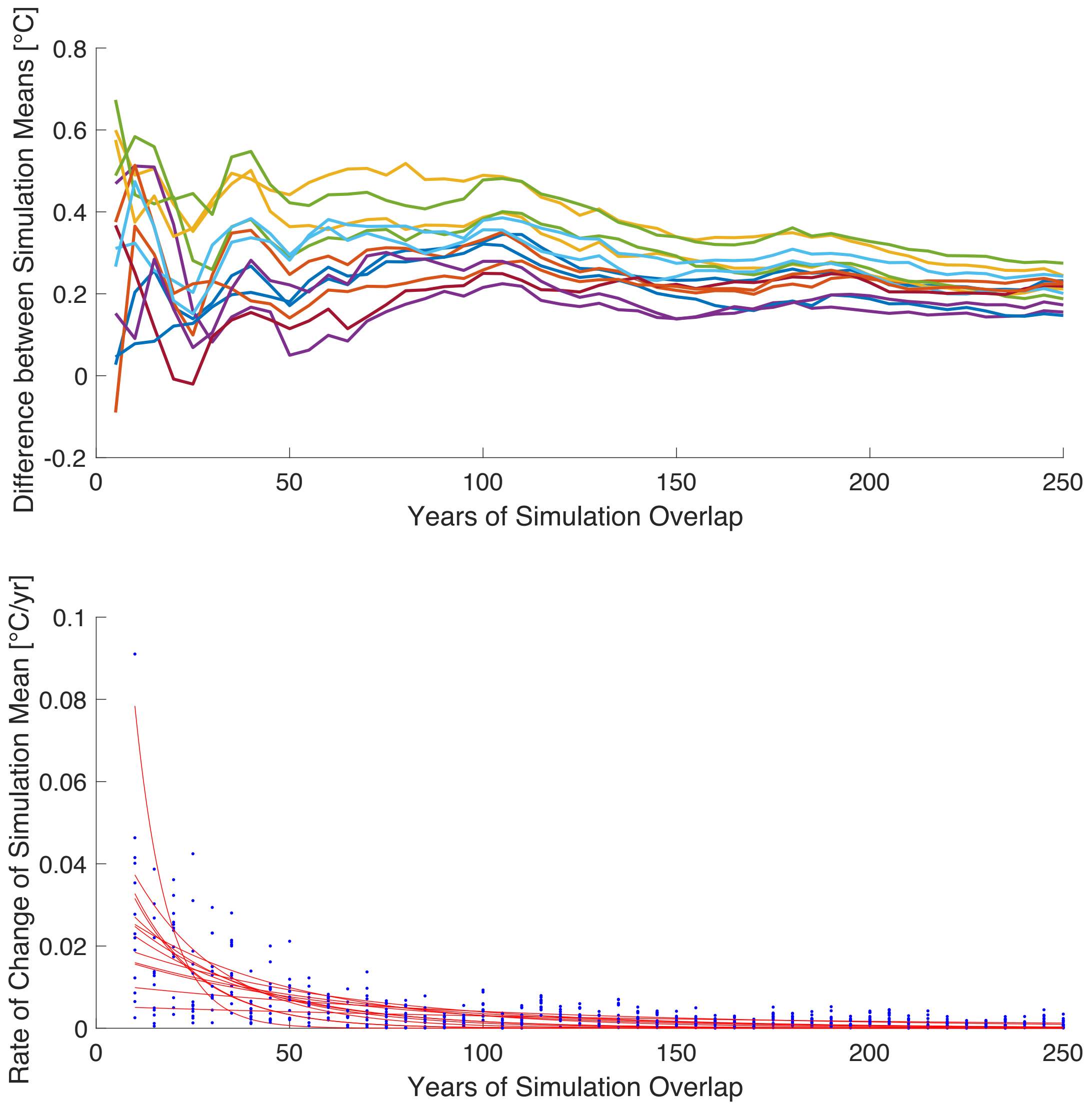

Figure 9: The top panel shows how the mean of LME simulations changes with increasing years of simulation overlap, approaching a mean value of ~0.21°C. The bottom panel shows the rate of change of the LME mean temperature with increasing year of overlap, and fitted exponential curves shows that change in the mean falls to 1% of the maximum after ~125 years of overlap.

Removal of the offset allows the two climate model simulations to be consolidated into a full 0-1850 CE run (combining our ongoing 0-1270 CE run with LME 12). From this composite, we can extract the mean temperatures from the first (0-1000 CE) and second millenniums (1000-1850 CE) and compare these to the 1 CE control conditions and also the temperatures derived from our DIC glacier model (Fig. 10). We find that the composite temperatures agree fairly well with our DIC glacier model which reported that, on average, the last ~2 ka had to have been ~.44°C cooler than 1 CE conditions.

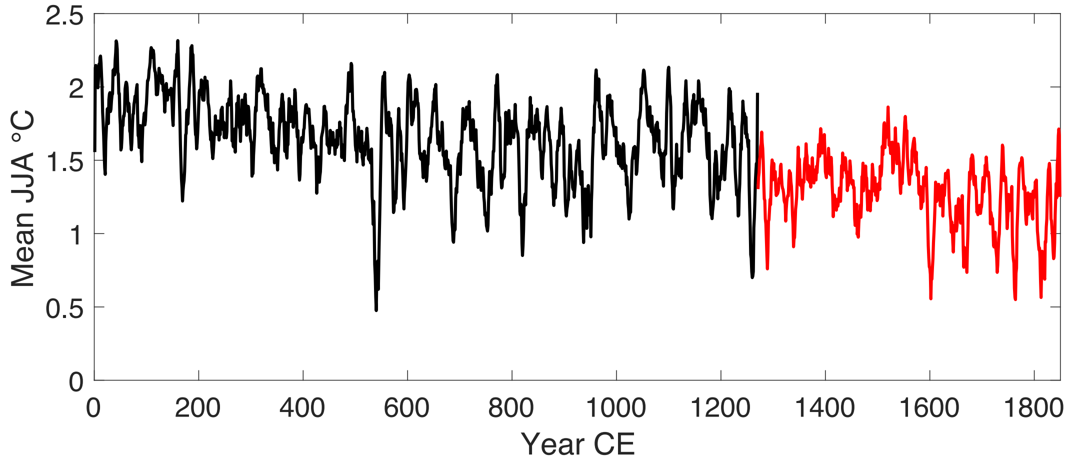

Figure 10:Plot of the composite simulated decadal temperatures (°C) for 60-90°N and 90°W-60°E, showing the ongoing past2K simulation in black (0-1270 CE) and the corrected LME Ensemble member 12 in red (1271-1850 CE).

References

Alley, R. B.: GISP2 ice core temperature and accumulation data, IGBP PAGES/World Data Cent. Paleoclimatology Data Contrib. Ser., 13, 2004.

Anklin, M., Bales, R. C., Mosley-Thompson, E. and Steffen, K.: Annual accumulation at two sites in northwest Greenland during recent centuries, J. Geophys. Res. Atmos., 103(D22), 28775–28783, doi:10.1029/98JD02718, 1998.

Benn, D. I. and Evans, D. J. A.: Glaciers and glaciation., 2010.

Braithwaite, R. J.: On glacier energy balance, ablation, and air temperature., J. Glaciol., 27(97), 381–391, 1981.

Braithwaite, R. J. and Olesen, O. B.: Calculation of glacier ablation from air temperature, West Greenland, Springer., 1989.

Cuffey, K. M. and Paterson, W. S. B.: The physics of glaciers, Academic Press., 2010.

Gardner, A. S., Sharp, M. J., Koerner, R. M., Labine, C., Boon, S., Marshall, S. J., Burgess, D. O. and Lewis, D.: Near-surface temperature lapse rates over arctic glaciers and their implications for temperature downscaling, J. Clim., 22(16), 4281–4298, doi:10.1175/2009JCLI2845.1, 2009.

Gearheard, S., Pocernich, M., Stewart, R., Sanguya, J. and Huntington, H. P.: Linking Inuit knowledge and meteorological station observations to understand changing wind patterns at Clyde River, Nunavut, Clim. Change, 100(2), 267–294, doi:10.1007/s10584-009-9587-1, 2010.

Haeberli, W.: Brief communication: On area- and slope-related thickness estimates and volume calculations for unmeasured glaciers, Cryosph. Discuss., (January), doi:10.5194/tc-2015-222, 2016.

Hock, R.: Glacier melt: a review of processes and their modelling, Prog. Phys. Geogr., 29(3), 362–391, doi:10.1191/0309133305pp453ra, 2005.

Hooke, R. L.: Pleistocene ice at the base of the Barnes Ice Cap, Baffin Island, NWT, Canada, J. 0/Glaciology, 17(75), 1976.

Jonsell, U., Navarro Valero, F. J., Bañón, M., Izargain, L., Jesús, J. and Otero García, J.: Sensitivity of a distributed temperature-radiation index melt model based on AWS observations and surface energy balance fluxes, Hurd Peninsula glaciers, Livingston Island, Antarctica, Cryosph., 6(3), 539–552, 2012.

Jungclaus, J. H., Bard, E., Baroni, M., Braconnot, P., Cao, J., Chini, L. P., Egorova, T., Evans, M., González-Rouco, J. F., Goosse, H., Hurtt, G. C., Joos, F., Kaplan, J. O., Khodri, M., Klein Goldewijk, K., Krivova, N., LeGrande, A. N., Lorenz, S. J., Luterbacher, J., Man, W., Meinshausen, M., Moberg, A., Nehrbass-Ahles, C., Otto-Bliesner, B. I., Phipps, S. J., Pongratz, J., Rozanov, E., Schmidt, G. A., Schmidt, H., Schmutz, W., Schurer, A., Shapiro, A. I., Sigl, M., Smerdon, J. E., Solanki, S. K., Timmreck, C., Toohey, M., Usoskin, I. G., Wagner, S., Wu, C.-Y., Yeo, K. L., Zanchettin, D., Zhang, Q. and Zorita, E.: The PMIP4 contribution to CMIP6 - Part 3: the Last Millennium, Scientific Objective and Experimental Design for the PMIP4 past1000 simulations, Geosci. Model Dev. Discuss., 2016, 1–34, doi:10.5194/gmd-2016-278, 2016.

Kane, D. L., Gieck, R. E. and Hinzman, L. D.: Snowmelt modeling at small Alaskan Arctic watershed, J. Hydrol. Eng., 2(4), 204–210, 1997.

Kessler, M. A., Anderson, R. S. and Stock, G. M.: Modeling topographic and climatic control of east-west asymmetry in Sierra Nevada glacier length during the Last Glacial Maximum, J. Geophys. Res. Earth Surf., 111(2), 1–15, doi:10.1029/2005JF000365, 2006.

Koerner, R. M.: Mass balance of glaciers in the Queen Elizabeth Islands, Nunavut, Canada, Ann. Glaciol., 42(1), 417–423, 2005.

Kumar, L., Skidmore, A. K. and Knowles, E.: Modelling topographic variation in solar radiation in a GIS environment, Int. J. Geogr. Inf. Sci., 11(5), 475–497, doi:10.1080/136588197242266, 1997.

Kustas, W. P., Rango, A. and Uijlenhoet, R.: A simple energy budget algorithm for the snowmelt runoff model, Water Resour. Res., 30(5), 1515–1527, doi:10.1029/94WR00152, 1994.

Lang, H. and Braun, L.: On the information content of air temperature in the context of snow melt estimation, IAHS Publ, 190, 347–354, 1990.

Lauriol, B., Carrier, Y., Beaudet, H. and Binda, G.: The residual snow cover in the Canadian Arctic in July: a means to evaluate the regional maximum snow depth in winter, Arctic, 39(4), 309–315 [online] Available from: http://www.jstor.org/stable/40511027, 1986.

Mair, D., Burgess, D. and Sharp, M.: Thirty-seven year mass balance of Devon Ice Cap, Nunavut, Canada, determined by shallow ice coring and melt modeling, J. Geophys. Res. Earth Surf., 110(1), 1–13, doi:10.1029/2003JF000099, 2005.

Marshall, S. J. and Sharp, M. J.: Temperature and melt modeling on the Prince of Wales Ice Field, Canadian high arctic, J. Clim., 22(6), 1454–1468, doi:10.1175/2008JCLI2560.1, 2009.

Nawri, N. and Stewart, R. E.: Climatological features of orographic low-level jets over frobisher bay, Atmosphere-Ocean, 44(4), 397–413, doi:10.3137/ao.440405, 2010.

Otto-Bliesner, B. L., Brady, E. C., Fasullo, J., Jahn, A., Landrum, L., Stevenson, S., Rosenbloom, N., Mai, A. and Strand, G.: Climate variability and change since 850 ce an ensemble approach with the community earth system model, Bull. Am. Meteorol. Soc., 97(5), 787–801, doi:10.1175/BAMS-D-14-00233.1, 2016.

Serreze, M. C., Rehder, M. C., Barry, R. G., Walsh, J. E. and Robinson, D. A.: Variations in aerologically derived Arctic precipitation and snowfall, Ann. Glaciol., 21, 77–82, 1995.

Williams, L. D.: The variation of corrie elevation and equilibrium line altitude with aspect in eastern Baffin Island, NWT, Canada, Arct. Alp. Res., 169–181, 1975.